Journal of Materials Science and Engineering A 8 (1-2) (2018) 32-42
doi: 10.17265/2161-6213/2018.1-2.005

Lead-Free Piezoelectric Ceramics as Candidates on the Development of Morphing Winglets in Aircrafts

Kevin Jiménez[1] and Guillermo Herrera[2]

1. Universidad Politécnica de Chihuahua, Av. Téofilo Borunda No. 13200 Col. Labor de Terrazas, 31220, Chihuahua, Chih. México

2. Cátedras CONACYT assigned to Centro de Investigación en Materiales Avanzados, Miguel de Cervantes 120, Complejo Industrial, 31136 Chihuahua, Chih. México

Abstract: In this paper we discussed the development of a morphing wingtip device or winglet for aircraft. The aim of this research is enhancing the aerodynamic of aircrafts, by optimizing the winglet shape, angle and torsion, to reduce wingtip vortices at each flight stage, reduce drag, fuel consumption and increase its endurance. The development of a working physical wingtip device with morphing functionality, is possible by using piezoelectric MFCs (Macro Fiber Composites) as actuators in wing structures. Due to their excellent properties like flexibility, light weight, tolerant to damage and long term stability MFC fit most of the requirements and specifications of morphing structures. Unfortunately, they are based on the toxic compound of $PbZr_xTi_{1-x}O_3$ (PZT). Lead-free materials can replace lead based compounds. Also, other aim of this inquiry is the development of piezoelectric lead-free compounds based on the solid solution $Ba_{1-x}Ca_xTi_{0.9}Zr_{0.1}O_3$ (BCZT) with x = 0.1, 0.125, 0.15. The reason for choosing these compositions is because BZCT compounds could reach a piezoelectricity coefficient d_{33}~400 pC/N. This value is comparable with commercial PZT, therefore it is a great candidate to replace it.

Key words: Piezoelectric, morphing plane, MFCs, vortices, winglet.

Nomenclature

CFD:	Computer fluid dynamics
MFC:	Macro fiber composite
SMA:	Shape-memory alloy
UAV:	Unmanned aerial vehicles
UAS:	Unmanned aircraft system
ISR:	Intelligence, surveillance and reconnaissance
Cant Angle:	Angle between the vertical and the winglet
V:	Airspeed (m/s-knots)

Greek Letters

α:	Angle of attack (°)
ρ:	Density (kg/m^3)
ν:	Kinematic viscosity (m^2/s)

1. Introduction

Morphing aircrafts are a new concept, the motivation to perform an inquiry about this technology is to enhance the aerodynamics of aircraft wings, as well to upgrade performance, reduce fuel consumption and provide a wide range of maneuverability. A wing in the process of generating lift develops strong vortices at wingtips. Wingtip vortices are caused by the pressure difference between the upper and lower sides of a lifting surface equalizing at the tip, as show in Fig. 1. This swirling flow leads to an aerodynamic drag component known as induced drag.

The drag breakdown of a typical transport aircraft shows that the lift-induced drag can amount to as much 40% of the total drag at cruise and more than 90% of the total drag at takeoff of a typical transport aircraft [1].

Aircraft winglets are wing vertical sections located at wingtips. The winglets therefore allow for a reduction of these vortices and so a reduction in lift induced drag [2]. Winglets fixed at a cant angle around 25°, can cut an aircraft's fuel consumption by

Corresponding author: Kevin Enrique Jiménez Mora, B. Eng., engineer, research fields: morphing aircrafts, unmanned aerial vehicles UAVs, micro aerial vehicles MAVs, lead free ferro-piezoelectric materials.

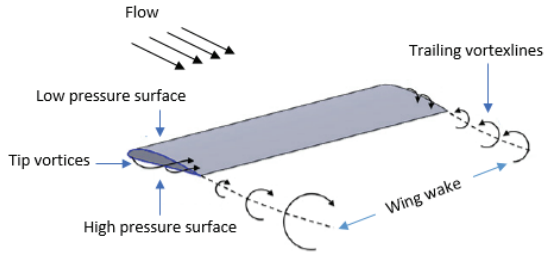

Fig. 1 Development of wingtip vortices by the lift, modified from reference [3].

3 to 5 percent. Winglets, are most commonly optimized to cruise flight but not at individual stages. This means that common winglets are obsolete at take-off, climb, initial cruise, final cruise and landing, therefore this means efficiency losses through its drag. The advantage of morphing winglets is that throughout the flight mission the aerodynamics of the wing can be optimized for each stage (take-off, climb, cruise, decent and landing). Boeing has filed a patent application on a winglet that moves using SMAs (Shape Memory Alloys) [4]. With elastic properties, whose shape can be temporarily changed by applying electrical currents, heat and pressure for example, later recover its original shape. But this mechanism needs much electrical power.

The characterization of a wingtip device for small aircrafts with morphing functionality is possible by using MFCs (Macro Fiber Composites) as actuators. Due to their excellent properties like flexibility, light weight, tolerant to damage and long term stability MFCs fit most of the requirements and specifications of morphing structures. MFCs were developed by the NASA and are presently manufactured and marketed by Smart Material Corporation [5].

Piezoelectric materials are well known for their high force, broad bandwidth actuation, and electrically induced small strains. The MFC consists of rectangular piezo ceramic rods sandwiched between layers of adhesive, electrodes and polyimide film. The electrodes are attached to the film in an interdigitated pattern which transfers the applied voltage MFC-structure directly to and from the ribbon shaped rods. This assembly enables in-plane poling, actuation and sensing in a sealed and durable, ready to use package. As a thin, surface conformable sheet can be applied (normally bonded) to various types of structures or embedded in a composite structure. If voltage is applied it will bend or distort materials, counteract vibrations or generate vibrations. If no voltage is applied it can work as a very sensitive strain gauge, sensing deformations, noise and vibrations. The MFC is also an excellent device to harvest energy from vibrations [5].

Unfortunately, they are made of the lead-based toxic compound $PbZr_xTi_{1-x}O_3$ (PZT). The research group of multiferroics in CIMAV Chihuahua is working on the development of lead-free ceramics with perovskite structure that shows ferroelectric and piezoelectric properties [6]. These materials are based on the solid solution $Ba_{1-x}Ca_xTi_{0.9}Zr_{0.1}O_3$ (BCZT) with x = 0.1, 0.125, 0.15. The reason for choosing these compositions is because BZCT compounds could reach a piezoelectricity coefficient d_{33}~400 pC/N around the same value of commercial PZT d_{33}~400 pC/N used in MFCs. Therefore, these compounds open the possibility of replacing lead-based compounds by lead-free compounds.

2. Experimental Setup

2.1 CFD Simulation

The model used is a wing similar as used in military UAVs. Those aircrafts have long endurance in order to provide military field commanders with comprehensive, near-real-time intelligence, surveillance and reconnaissance (ISR), plus detection of moving targets over a large geographical area for battle management, targeting and situation awareness of enemy actions.

NASA LRN 1015 is shown in Fig. 2. Airfoil was chosen for both the wing section and the winglet. Airfoil used on the Northrop Grumman RQ-4 Global Hawk, is a high-altitude, long-endurance UAS. The wing model geometry was also inspired on the Northrop Grumman RQ-4 in Fig. 3.

Fig. 2 NASA LRN 1015. Max thickness 15.2% at 40% chord. Max camber 4.9% at 44% chord, modified from reference [7].

Fig. 3 Global Hawk RQ-4; top: RQ-4 flying; bottom: RQ-4 size (40 m RQ-4B wingspan, 35 m RQ-4A wingspan) [10, 11].

This aircraft was chosen because it performs as a ceiling service around 60,000 feet (18 km) and an endurance above 32 hours. Thus, its performance can be optimized by the use of wingtip devices with morphing functionality using MFCs as actuators reducing the fuel consumption at climb and descent stages therefore giving extra-hours of endurance. The design parameters for the base model used in the CFD study are given in Table 1.

The wing models were designed and analyzed at the software XFLR5 version 6.38. XFLR5 is an analysis tool for airfoils, wings and planes [8, 9]. Three wing models were designed to ascertain the performance of each wing in Fig. 4; wing without winglet in Fig 4a; fixed winglet wing with a cant angle of 30° in Fig. 4b; morphing MFC actuated winglet wing in Fig. 4c.

Table 1 Design parameters of the wing and winglet.

Parameter	Wing	Winglet
Half span	17.5 m	2 m
Root chord	2.25 m	0.8 m
Tip chord	.8 m	0.4 m
Taper ratio	3.8	2
Sweep angle	7°	11.3°
Airfoil	LRN 1015	LRN 1015

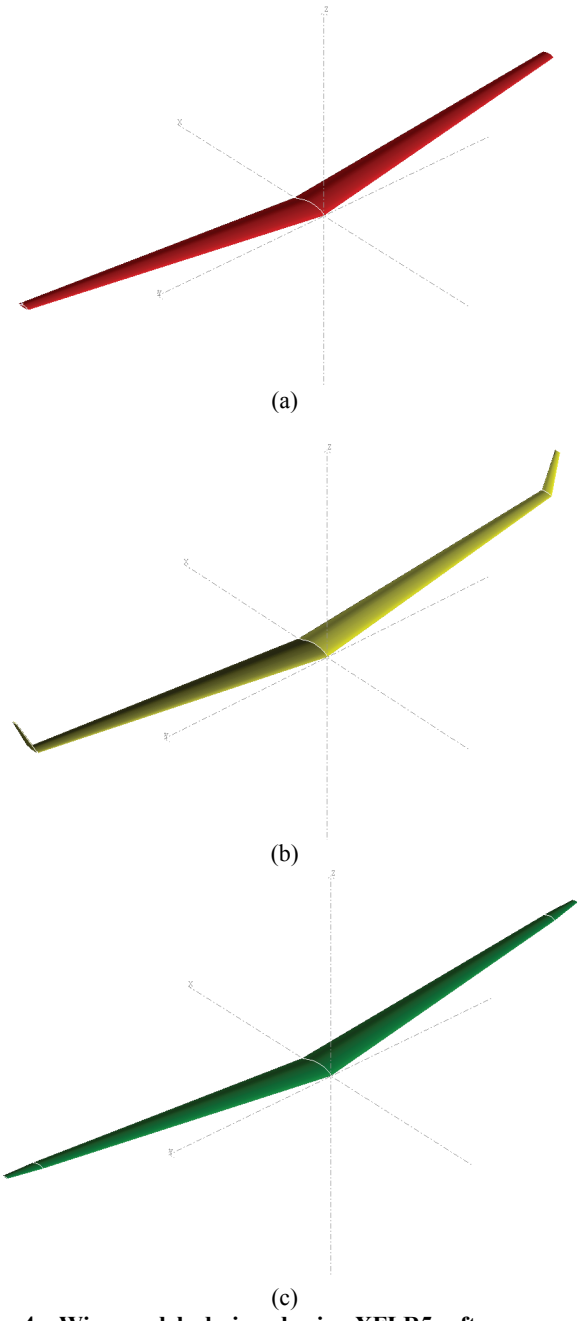

(a) (b) (c)

Fig. 4 Wing models designed using XFLR5 software.

The three different wings were analyzed at different speeds and angles of attack in order to compare the performance of each wing (Fig. 4). The parameters for the CFD study were airspeed of 100 m/s, density ρ at sea level of 1.225 kg/m^3 and kinematic viscosity ν of 1.5e-05 m^2/s.

2.2 Experimental Procedure

Piezoelectric $Ba_{1-x}Ca_xTi_{0.9}Zr_{0.1}O_3$ (BCZT) ceramics was prepared with x = 0.1, 0.125, 0.15 by modified Pechini method. The reason for choosing these compositions is because Liu et al. [12] reports compounds of BZT and BCT with a piezoelectricity coefficient d_{33}~600 pC/N, similar value to the piezoelectricity coefficient d_{33} of the MFC of 460 pC/N. This device operates in a range of -500 V to +1,500 V and the currents for its operation are of the order of milliamps. The MFCs are typically flexible, tolerant damage although many of them are based on the toxic compound of $Pb(Zr_xTi_{1-x})O_3$. Fig. 5 presents the design of a MFC.

The compound was prepared by the modified Pechini method in Fig. 6. The starting materials used to prepare the BCZT compound by the Pechini polymeric precursor method were: $Ba(NO_3)_2$ (Alfa Aesar, 99.999%); $Ca(NO_3)_2{\cdot}4H_2O$ (J. T. Baker, 99.9%); $Zr(C_5H_8O_2)_2$ (Aldrich, 98.5%) $TIO(C_5H_8O_2)_2$ (Sigma-Aldrich, 95%); ethylenediaminetetraacetic acid, EDTA (Alfa Aesar, 99%); NH_4OH (Fermont, 66%); citric acid $C_3H_4(COOH)_3{\cdot}H_2O$ (J. T. Baker, 99.5%) and ethylene-glycol $C_2H_6O_2$ (J. T. Baker, 99.9%).

In the first stage of the experiment, to prepare 0.5 g of Ba-Ca-Ti-Zr-O precursor, 0.516 g of $Ba(NO_3)_2$ was dissolved into 100 mL of distilled water for 15 min under magnetic stirring at 60 °C. In order to avoid the precipitation of $Ba(NO_3)_2$, or to form complexes, the chelant agent EDTA was used to isolate the Ba cation, then 2.8 g of EDTA was added to this solution maintaining uninterrupted stirring.

Dripping appropriate amount of ammonia was used to obtain a transparent solution with pH 8. Then 0.051 g

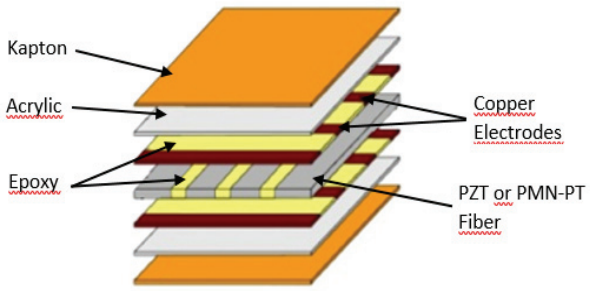

Fig. 5 MFC layers, modified from reference [13].

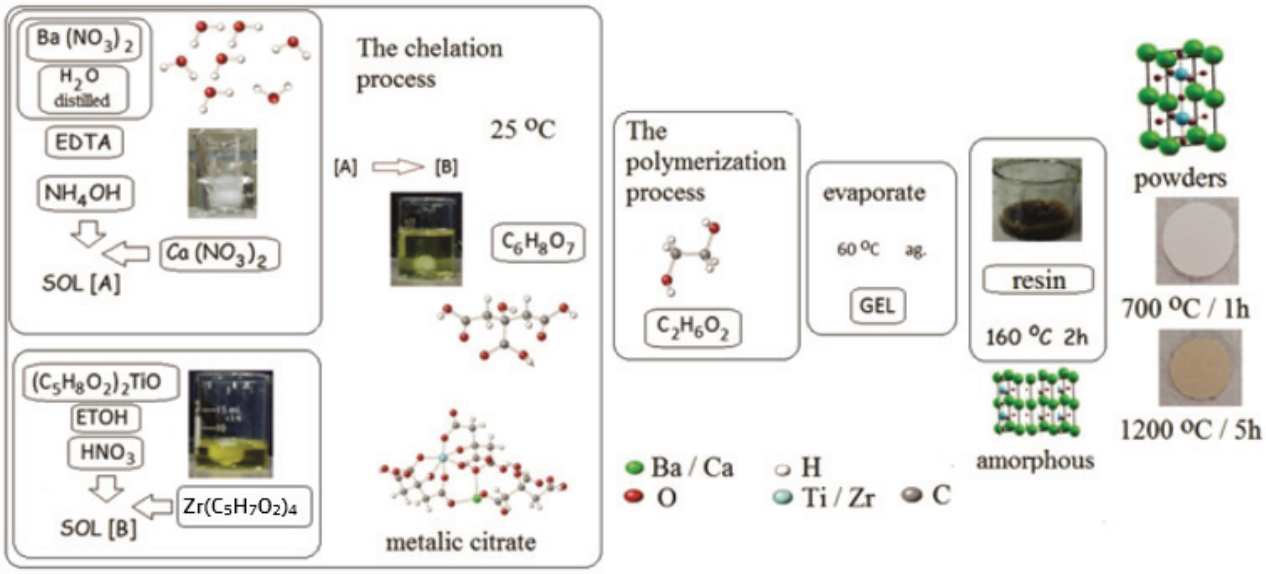

Fig. 6 Flow chart for the modified Pechini method used to prepare the BCZT.

of $Ca(NO_3)_2 \cdot 4H_2O$ was added to this solution. This transparent solution is marked as solution A. Then 0.483 g of $TIO(C_5H_8O_2)_2$ was disperse in 30 mL of ethanol (Aldrich) during 5 min at 60 °C. NHO_3 was added until a transparent yellow solution was obtained. Then 0.115 g of $Zr(C_5H_8O_2)_2$ was added, this solution is marked as solution B maintaining uninterrupted stirring at 25 °C. Immediately, the chelant agent of citric acid and ethylene-glycol (to induce the polymerization) in a 3:1 M ratio were incorporated to the above solution. Then, this solution was stirred at room temperature for 10 min.

The mixture was heated at 60 °C at the same time the pH value was adjusted to be 4 using ammonia till a transparent liquid was achieved. Followed by a continuous stirring for 2 h at 60 °C for evaporating solvents, the viscosity of solution increased gradually. After 2 h a stable transparent yellow gel was formed. This gel was heated at 160 °C during 2 h using a heating rate of 5 °C/min and milled for obtaining a dark-brown resin.

The resin was heat treated at 700 °C during 1 h using a heating ratio of 10 °C/min and milled for 15 min. White powders were obtained that were pressed into pellets of 7.68 mm diameter and thickness of 1 mm. Then, the pellets were sintered at 1,200 °C for 5 h and 1,275 °C during 5 h. The flow chart of the procedure mentioned above is showed in Fig. 6.

3. Results

3.1 CFD Results

Fixed cant angle wingtip devices are optimized while cruise flight but not at individual stages, thus, these devices are obsolete at the climb and descent stages. Fig. 7 shows the comparison between a conventional wing (Figs. 7a-7b) and a wing with fixed cant angle winglet of 30° (Figs. 7c-7d). Flying at the same speed at cruise $\alpha = 0°$ (Figs. 7a-7c) the wing without winglet creates few vortices and the fixed winglet reduces the vorticity. But while climbing $\alpha = 30°$ in Figs. 7b-7d both wings have the same performance creating large vortices.

With a morphing MFC actuated wingtip device is possible to reduce the vorticity at each flight stage. Figs. 7e-7f show the performance of two wings with morphing winglet; Fig. 7e shows how just increasing the cant angle to 75° is possible to reduce the vorticity climbing at the same angle of 30°, same value than the fixed winglet and without winglet wing, drastically reducing vorticity.

Also, the vorticity can be reduced more by twisting the winglet tip few degrees as Fig. 7f shows a wing with winglet that has a cant angle of 105° and a twisting of -15° at the tip; taking as positive the upper surface of the wing and negative the lower surface of the wing. This configuration reduces vorticity even better than Fig. 7e model where the vorticity starts early almost at wingtips in comparison with Fig. 7f model.

The simulations shown results of variating the cant angle and twist of a winglet, enhancing the performance in order to reduce drag vortices at climb and descent stages. By bending and twisting the winglets those results were obtained that are the work modes of the MFCs actuators in Fig. 8.

Also, it is possible to achieve better results by variating other parameters of the winglet at flight using these devices by its work modes in Fig. 9. These devices can be commercially manufactured to a max. size of 40 cm by 53 cm, 15.7 inches by 20 inches [5] enough for the RQ-4 by its wingtip chord around of 80 cm, 31 inches, and for other aircrafts using more than one actuator each wingtip.

3.2 Material Results

The most relevant results of the material characterization are: structurally stabilizing the tetragonal crystal phase at low temperatures 650-700 °C, as the thermal analysis and differential scanning calorimetry pattern of X-ray diffraction, XRD Figs. 10a-10c from an amorphous phase in Fig. 10b.

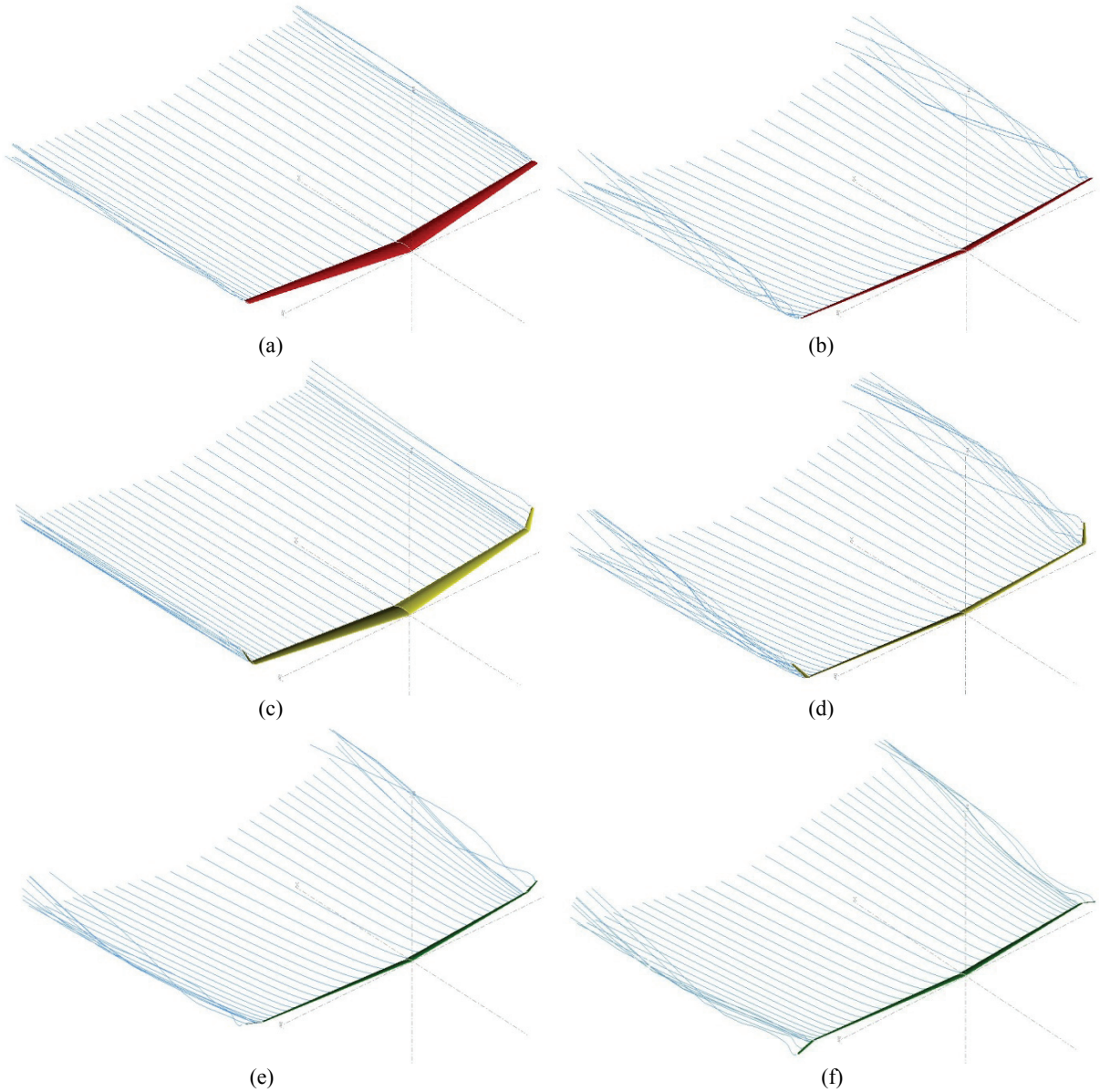

Fig. 7 CFD analysis of wing models using XFLR5 software.

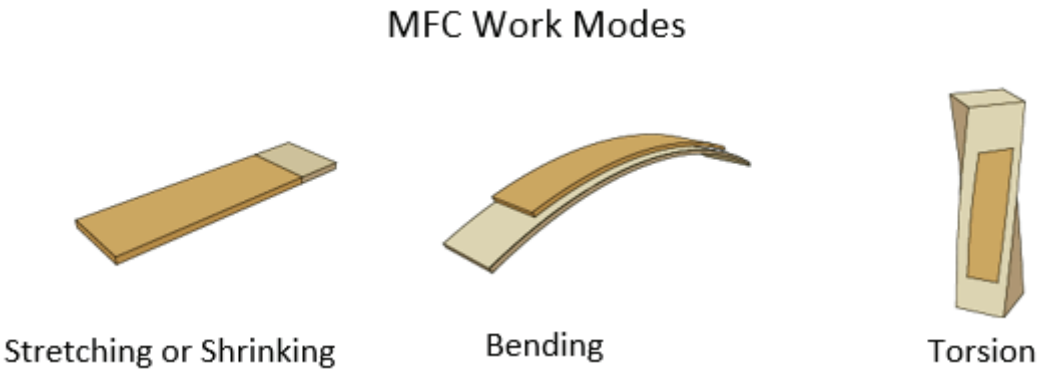

Fig. 8 Macro fiber composite actuators work modes, modified from reference [5].

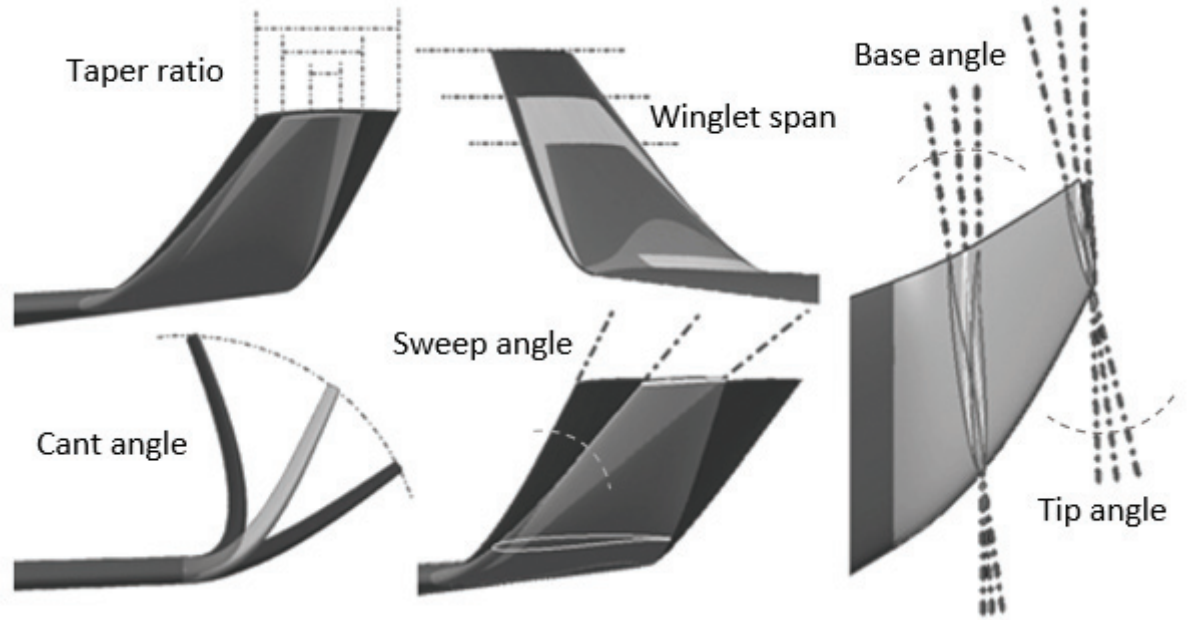

Fig. 9 Winglet design parameters, modified from reference [16].

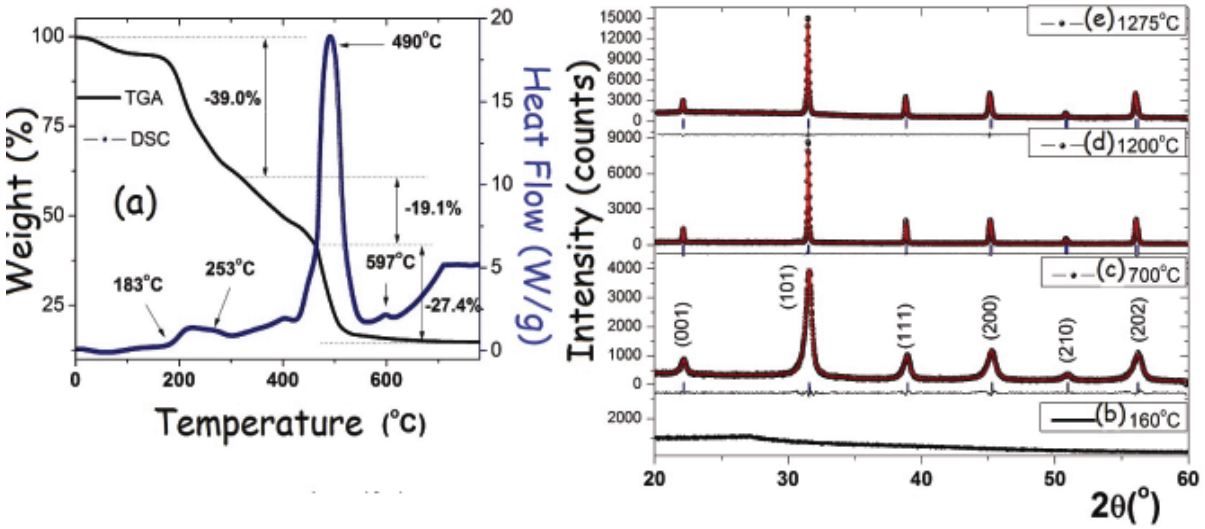

Fig. 10 Thermal analysis: thermogravimetry and differential scanning calorimetry and structural evolution monitored by XRD.

Once the crystalline phase was stabilized, in order to promote a better material densification it is milled in a high-energy mill (1 h 30 min). The resulting powder is compacted in tablet form and sintered to 1,200 °C shown in Figs. 10d-10e and 1,275 °C for 5 h. The interpretation of these XRD patterns was performed by using the refinements by the Rietveld method using Fullprof software [14, 15].

With this study the evolution of lattice parameters and crystal size (Scherer Equation) was elucidated. The tetragonal crystal phase (P 4mm space group) was also considered in accordance with the JCPDS 81-1066 tab. Refinement for the sample at 1,275 °C in Fig. 10e was improved by including 52% of the crystalline phase rhombohedral (R3c) and 48% of the tetragonal phase [17, 18].

The piezoelectric hysteresis cycles were determined by force-microscopy of the PFM (piezo-response) method [19, 20]. It was operated in vertical mode with an AC voltage amplitude of 5 V pk-pk and a

conduction frequency of 295 kHz remote from the resonance frequency of the cantilever, the local polarization (hysteresis cycles), a voltage of -15 to 15 V pk-pk was applied by the Dual AC (DART) resonance tracking method.

Fig. 11 shows a comparison between the ferroelectric behavior through the hysteresis cycles of amplitude (b), phase (c) and piezoelectric coefficient d_{33} (d) as a function of the AC potential applied to the samples at 700 °C (Particles on the nanoscale) and 1,275 °C (grains on the micron scale) represents the active area of the piezo-response.

The amplitude (pm) as a function of the AC (V) potential presents a butterfly-shaped cycle and contains piezoelectric deformation information [21]. The phase (°) as a function of the potential AC (V), demonstrates the polarization change [22]. This result confirms the polarization change due to a potential, establishing the presence of domains of 180 ° in the nanocrystals [23, 24].

From the amplitude curves the local piezoelectricity coefficient d_{33} is determined and this is done through the following expression:

$$(V - V_1)d_{33} = D - D_1$$

where D is the value of the piezoelectric strain or amplitude, V is the applied potential, D_1 and V_1 are the piezoelectric deformation and the potential applied at the intersection of the butterfly [22].

The sample treated at 700 °C has a d_{33} of 8.25 pm/V at a maximum potential of 15 V. The coercive potential (1.64 V) was determined using the expression $(Vc^+ - Vc^-)/2$ where Vc^+ and Vc^- are the direct and reverse coercive potentials. The d_{33} obtained for the sample treated at 1,275 °C is 110 pm/V at a maximum potential of 15 V. The coercive potential is 2.24 V.

Fig. 12 (a, b) presents the AFM topography images of BCZT powders obtained under the two different heat treatments. Both micrographs show that the powders have presence of small porosity. The micrograph (a) for the sample heated at 700 °C during 1 h confirmed the homogeneus particle shape and size distribution, the last one centered at 30 nm. The roughness analysis was performed using the software presented in Ref. [25] on an area of 1 × 1 μm^2 for these powders have a RMS (root-mean-square) roughness of 16.7 nm and roughness average (Ra) of 11.7 nm. In comparison, the roughness analysis on an area of 20 × 20 μm^2 for powders obtained at 1,200 °C during 5 h (b) has a dense surface, with a heterogeneous grain shape distribution that exhibits polyhedral-shape (RMS roughness is 1.3 μm and Ra= 1.0 μm).

Piezoelectric coefficient d_{33} was 45 pC/N for the sample heated at 1,200 °C and 140 pC/N for the sample heated at 1,250 °C. Ferroelectric hysteresis loops measured at room temperature is shown in Fig. 12c a low coercivity, “soft” P-E loops, in both samples were determined (EC) = 0.5 kV/cm with a

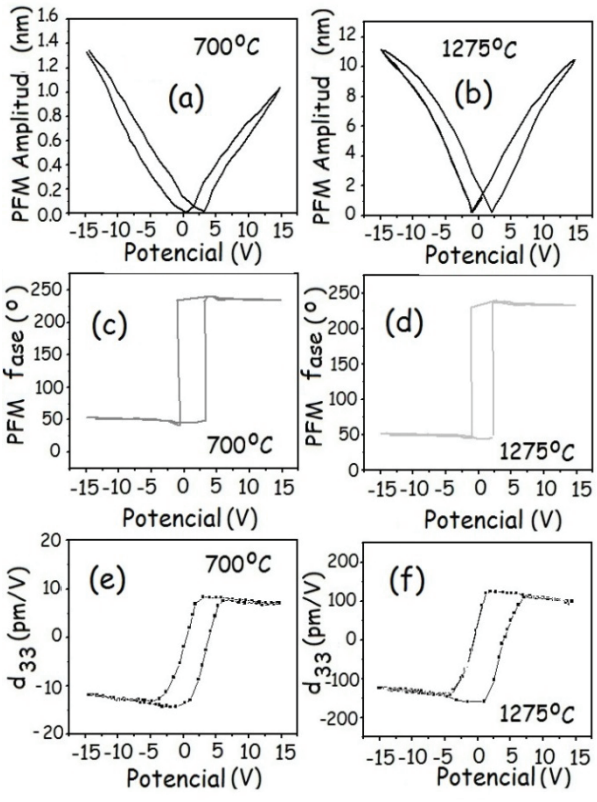

Fig. 11 Comparison between the curves of: amplitude (a-b) phase (c-d) piezo-response (d_{33}) (e–f) as a function of the AC potential applied to the thermally treated BCZT pellets at 700 °C for 1 h and 1,275 °C for 5 h.

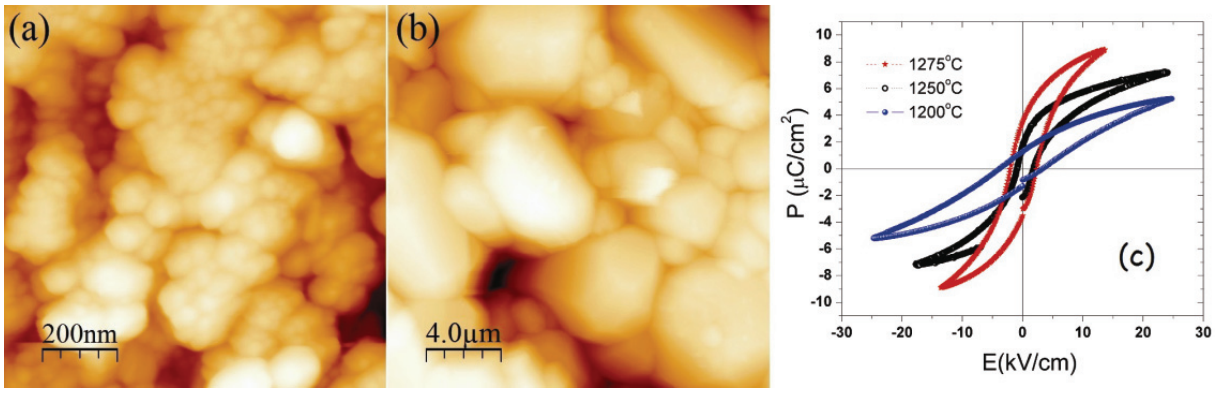

Fig. 12 AFM comparison between (a) (b) (c) Polarization-electric field hysteresis loops measured at room temperature for the sample heated at 1,200 °C 5h.

remanent polarization of 2.1 μC/cm^2 for the sample heated at 1,200 °C and 4.2 μC/cm^2 for the sample heated at 1,250 °C.

These measurements were performed at room temperature. Low values could be attributed to the low densities values obtained during sintering process, low voltage and time values during poling process.

4. Conclusions

Based on the results obtained it is possible to affirm that morphing wingtip devices save millions of dollars by the reduction of fuel consumption optimizing wingtips at each flight stage, as the computer fluid dynamics studies showing variating winglet design parameters based on the MFCs work modes we obtained excellent results as a reduction of the vorticity amounting to almost a laminar flow, climbing at high speed of 100 m/s and an angle of attack of 30°.

Conventional winglets are optimized for cruise flight; aircrafts performance, cruise speed, is basically the speed at which the wing airfoil develops less drag. This fact lead us to keep working to obtain same results at every single flight stage, this would increase aircrafts autonomy like no other device, considering that the lift-induced drag can amount to as much 40% of the total drag at cruise and more than 90% of the total drag at takeoff of a typical transport aircraft [1], by flying at almost zero drag conditions. The RQ-4 Global Hawk has an autonomy of 36 h without any wingtip device; flying at almost zero drag the RQ-4 could reach an autonomy above 40 h.

This technology is profitable for being applied in almost every kind of aircraft, military and commercial aviation, this opens the possibility of non-stop commercial flights, extra flight time and area cover of rescue aircrafts and extended flight time and range of maneuverability in military aircrafts. This technology could be applied as other devices as flaps, ailerons, rudders and elevators, maybe in a future by the use of composites and light alloys in aircrafts structures, high strength hydraulic actuators could become useless, comparing with MFCs, that represents an insignificant weight, being integral part of the structure, reducing weight, drag, crating better aerodynamic surfaces, allowing reducing the amount of thrust which would give way to the use of smaller or even electric motors which in both cases would be a considerable reduction of CO_2 emissions to the environment.

Lead-free perovskite BCZT compound has been successfully synthesized by a Pechini polymeric precursor method. The piezoelectric coefficient d_{33} and the polarization limits obtained by ferroelectric loops analysis are slightly lower than those showed at the literature. The microstructure reveals polygon-shape distribution with the presence of inter-grain porosity. These results could be attributed to different factors as the low densification of the material when we stabilized the tetragonal crystal phase at 700 °C, low time and DC poling voltage

around 5,000 V for 24 h, we obtained d_{33} values around 140 pC/N, comparing with PZT d_{33} values around 450 pC/N of the MFCs that are treated at DC poling values of 15,000 V and probably for a time above 48 h; these results motivate us to continue with this research, it has been shown that it is possible to obtain a lead-free piezoelectric ceramic in bulk, lead-free that presents ferroelectric properties, through the Pechini method, viable, reproducible, manageable and affordable. This opens the possibility to replace toxic lead based compounds of PZT by BCZT lead-free compounds in devices as MFCs for aeronautical applications as the development of morphing winglets.

Acknowledgments

The authors would like to express thanks to the CONACyT-SEP Basic Research Project 2015 No. 253605. K. Jiménez also to express gratitude to M.E. J. Minjarez Enríquez who gives some advices on computer fluid dynamics analysis. G. Herrera-Pérez would like to thank for complementary support SNI I-CONACyT. The authors also would like to express gratitude to M.Sc. D. Lardizabal-Gutiérrez, M.Sc. E. Guerrero-Lestajette and M.Sc. O. Solis-Canto from the Laboratorio Nacional de Nanotecnología (NaNoTeCh).

References

[1] Gavrilović, N. N., Rašuo, B. P., Dulikravich, G. S.,Parezanović, V. B. 2015. "Commercial Aircraft Performance Improvement Using Winglets." *FME Transactions* 43 (1): 1.

[2] Whitcomb, R. T. NASA Technical Note. "A Design Approach and Selected Wind Tunnel Results at High Sub-sonic Speeds for Wingtip Mounted Winglets." July 1976, Report number: NASA TN D-8260.

[3] Guha, T. K., Oates, W., and Kumar, R. 2015 "Characterization of Piezoelectric Macrofiber Composite Actuated Winglets." *Smart Mater Struct* 24 (6): 065043.

[4] United States. Patent Application Publication Sankrithi et al. Pub. No.: US2008/0308683 A1. Dec. 18, 2008.

[5] Smart Material Corp., Sarasota (FL) USA. www.smart-materials.com.

[6] Herrera, G., Morales, D., Paraguay-Delgado, F., Borja-Urby, R., Reyes-Rojas, A., and Fuentes-Cobas, L. E. 2016. "Structural Analysis, Optical and Dielectric Function of $[Ba_{0.9}Ca_{0.1}](Ti_{0.9}Zr_{0.1})O_3$ Nanocrystals." *J. Appl. Phys.* 120 (9): 094303.

[7] Airfoil Tools. airfoiltools.com/airfoil/details?airfoil=lrn1015-il.

[8] http://www.xflr5.com/xflr5.htm.

[9] F., Meschia. 2008. "Model Analysis with XFLR5." *Radio Controlled Soaring Digest* 25 (2): 27.

[10] Northrop Grumman. http://www.northropgrumman.com/MediaResources/Pages/Photo.aspx?pid%3DGL-10001_067%26rel%3D%2F%26name%3DPhotos.

[11] Northrop Grumman. http://www.northropgrumman.com/MediaResources/Pages/Photo.aspx?pid%3DGH-10021_041%26rel%3D%2F%26name%3DPhotos.

[12] Liu, W., and Ren, X. 2009. "Large Piezoelectric Effect in Pb-Free Ceramics." *Phys. Rev. Lett*. 103: 257602.

[13] Park, J. S., and Kim, J. H. 2005. "Analytical Development of Single Crystal Macro Fiber Composite Actuators for Active Twist Rotor Blades." Smart Materials and Structures, 14 (4): 745.

[14] Rodriguez-Carvajal, J. 1993. "Recent Advances in Magnetic Structure Determination by Neutron Powder Diffraction." *Physica B*. 192: 55.

[15] Rodriguez-Carvajal, J., and Roisnel, T. 1998. "Commission on Powder Diffraction, International Union of Crystallography." *Newsletter* 20: 35.

[16] Cella, U., and Romano, D. G. 2010. "Assessment of Optimization Algorithms for Winglet Design." Engin Soft-Newsletter 7 (1): 6.

[17] Herrera-Pérez, G., Reyes-Rojas, A., Paraguay-Delgado, F., Fuentes-Cobas, L. E. 2015. en: Sánchez-Vázquez M., Sánchez-Castro M. E., Fernández-Luqueño F. (Eds.). "Encuentro de Química Inorgánica (EQI-2015)." Cinvestav, México, pp. 749-54.

[18] Herrera-Pérez, G., Castillo-Sandoval, I., Solis-Canto, Tapia-Padilla, G., Reyes-Rojas, A., and Fuentes-Cobas. L. E. 2018. "Local Piezo-Response for Lead-Free $Ba_{0.9}Ca_{0.1}Ti_{0.9}Zr_{0.1}O_3$ Electro-Ceramic by Switching Spectrosocopy." *Mater. Research in Press.* doi.org:10.1590/1980-5373-mr-2017-0605.

[19] Bharathi, P., Thomas, P., and Varma, K. B. R. 2015. "Piezoelectric Properties of Individual Nanocrystallites of $Ba_{0.85}Ca_{0.15}Zr_{0.1}Ti_{0.9}O_3$ Obtained by Oxalate Precursor Route." *J. Mater. Chem. C* 3: 4762.

[20] Herrera-Pérez, G., Solis-Canto, O., Holguin-Momaca, J., Olive-Mendez, S. Guerrero-Lestarjette, E., Tapia-Padilla, G., Reyes-Rojas, A., and Fuentes-Cobas. L. E. 2017. "Microstructure Patterns by Switching Spectroscopy Piezo-response Force Microscopy of Lead Free

Perovskite-type Polycrystalline Thin Films." *Microsc. Microanal.* 23 (suppl 1): 1648.

[21] Chen, Z., Huang, J., Yang, Y., Wang, Y., Wu, Y., He, H., Wei, X., Ye, Z., Zeng, H., Cong, H., and Jiang, Z. 2012. "Piezoelectric Properties of Rhombic $LiNbO_3$ Nanowires." *RSC Adv*. 2: 7380.

[22] Roelofs, A., Schneller, T., Szot, K., and Waser, R. 2003. "Towards the Limit of Ferroelectric Nanosized Grains." *Nanotechnology* 14:250.

[23] Kang, H. B., Chang, J., Koh, K., Lin, L., and Cho, Y. S. 2014. "High Quality Mn-Doped (Na,K)NbO_3 Nanofibers for Flexible Piezoelectric Nanogenerators." *ACS Appl. Mater. Interfaces* 6: 10576.

[24] Mohanty, D., Chaubey, G. S., Yourdkhani, A., Adireddy, S., Caruntu, G., and Wiley, J. B. 2012. "Synthesis and Piezoelectric Response of Cubic and Spherical $LiNbO_3$ Nanocrystals." *RSC Adv.* 2: 1913.

[25] Horcas, I., Fernández, R., Gómez-Rodríguez, J. M., Colchero, J., Gómez-Herrero, J., and Baro, A. M. 2002. "WSXM: A Software for Scanning Probe Microscopy and a Tool for Nanotechnology." *Rev. Sci. Instrum.* 78: 013705.